Photon–Free-Electron Interaction

Contents

Abstract

The interaction of photons with free electrons or holes in the respective bands strongly influences optical absorption and reflection in the spectral region between the absorption edge and the Reststrahlen wavelength. In a driving external field, the ensemble of free electrons (or, at higher frequency, of valence-electrons) oscillates with respect to the ion cores on the whole, leading to a plasma resonance absorption. The plasmon dispersion has two branches with frequencies depending on the carrier density. Nonresonant carrier absorption occurs away from the resonance, with a free-electron contribution predominantly from indirect transitions within the conduction band, and prevalent direct transitions for holes. The spectra and underlying dispersion relations provide valuable information about the effective masses of electrons and holes, carrier concentrations, and carrier-relaxation times.

K.W. Böer, U.W. Pohl, *Semiconductor Physics*,
https://doi.org/10.1007/978-3-319-69150-3_12

Keywords
Cyclotron-resonance absorption · Electron-plasma absorption · Faraday effect · Free-carrier absorption · Free-electron dispersion · Magnetoplasma reflection · Photon-free-electron interaction · Plasma frequency · Plasmon · Plasmon dispersion · Valence-electron plasma absorption

1 Free-Electron Resonance Absorption

The optical excitation of electrons or holes within their respective bands may involve a large variety of excitation mechanisms and multiparticle influences during the excitation process, such as:

- Direct (vertical in **k** space) transition from one into another branch of the same band
- Indirect transition with phonon assistance
- Transitions followed by other inelastic scattering processes
- Transitions involving collective effects of electrons (plasmons)
- Transitions between subbands created by a magnetic field

These processes will be discussed in the following sections. The treatment is quite similar to that applied to lattice vibrations discussed in chapter ► "Photon–Phonon Interaction". Collective electronic resonances and single-particle excitations can be well described in such classical model. The dielectric function of free electrons is similar to that of optical lattice vibrations, except that here the eigenfrequency is zero and the damping processes of the related optical absorption require a quantum-mechanical treatment.

The interaction of photons with free electrons in the conduction band or holes in the valence band can result in *resonant* or *nonresonant* absorption. Resonant absorption is discussed first because of the similarities in the mathematical treatment with the ionic oscillations. The logical extension of the field-induced lattice oscillation is the polarization of the *electronic shell* surrounding each lattice atom in an external electromagnetic field. In a classical model, the shift of the electron cloud with respect to the nucleus is proportional to the electric field and given by the electronic polarizability α_{el}. The resulting dispersion formula is similar to Eq. 42 in chapter ► "Photon–Phonon Interaction", except for a different eigenfrequency and damping factor relating to the electronic shell. When the electron density is large enough, such electron-collective effects cause resonance absorption, which for semiconductors lie in the IR range beyond the band edge.

1.1 Electron-Plasma Absorption

In an external electric field, the electrons act jointly when they are shifted as an entity with respect to the ionized donors. The field E_x exerts a force $-eE_x$ and

causes a shift by Δx from their on-the-average neutral position, creating a net charge at the two outer surfaces of the solid, which can be calculated by integrating the Poisson equation

$$\delta E_x = \frac{\rho}{\varepsilon\,\varepsilon_0}\Delta x = \frac{ne}{\varepsilon\,\varepsilon_0}\Delta x, \tag{1}$$

where n is the concentration of free electrons. The induced field δE_x counteracts the driving field E_x; that is, $e\delta E_x$ acts as restoring force, causing oscillations of the electron collective, following the equation of motion (Pines 1999):

$$n m_n \frac{d^2\Delta x}{dt^2} + n m_n \gamma \frac{d\Delta x}{dt} = -n\ e\,\delta E_x = -\frac{n^2\ e^2}{\varepsilon_{\text{opt}}\,\varepsilon_0}\Delta x; \tag{2}$$

m_n is the effective mass of a free electron, and γ is a damping parameter which can be related to an energy-relaxation time of electrons by $\gamma = 1/\tau_{\text{el}}$. We have introduced for ε the optical dielectric constant ε_{opt}, since we expect oscillations between the band edge and the Reststrahl frequency. With a driving external field, this equation can be modified as a damped harmonic oscillator equation (similar to Eq. 32 in chapter ▶ "Photon–Phonon Interaction")

$$m_n\left(\frac{d^2\Delta x}{dt^2} + \gamma\frac{d\Delta x}{dt} + \omega_p^2\Delta x\right) = eE_x\exp(-i\omega t). \tag{3}$$

ω_{p} is the *plasma frequency* obtained by comparing (Eqs. 2 and 3):

$$\omega_{\text{p}} = \sqrt{\frac{n\,e^2}{\varepsilon_{\text{opt}}\,\varepsilon_0\,m_n}}. \tag{4}$$

ω_{p} is the frequency at which an undamped plasma of electrons and positive ions oscillate on the whole in a longitudinal mode; this mode interacts strongly with electrons. There is also a transverse oscillation which interacts with electromagnetic radiation.

The restoring force in the motion of the electron plasma is proportional to the square of the plasma frequency. As a quantum of quantized energy, $\hbar\omega_{\text{p}}$ is referred to as a *plasmon*:

$$\hbar\omega_{\text{p}} = 38.9 \times \sqrt{\frac{n\,(\text{cm}^{-3})}{10^{16}}\,\frac{10}{\varepsilon_{\text{opt}}}\,\frac{m_0}{m_n}}\,(\text{meV}). \tag{5}$$

Plasmons can be observed directly by IR spectroscopy or Raman scattering, when the density of free carriers exceeds $\sim 10^{15}$ cm^{-3}. Raman spectra of undoped GaAs show for the backscattering geometry applied for Fig. 1 a strong

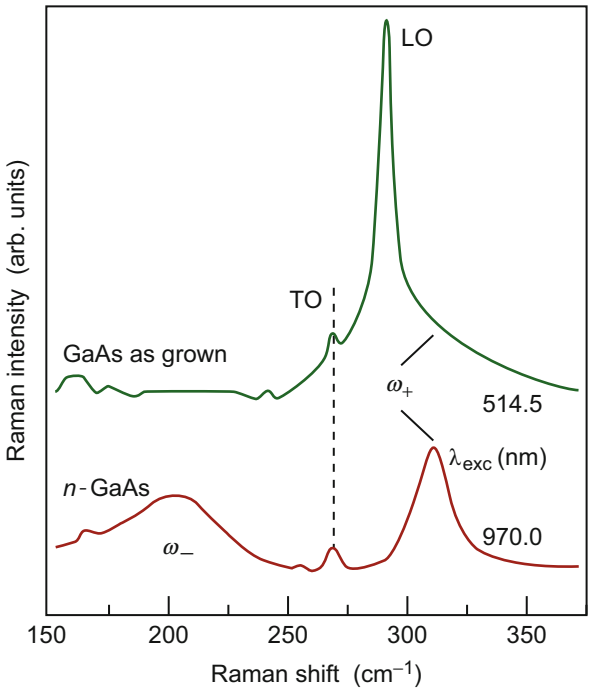

Fig. 1 Plasmon modes ω_- and ω_+ in the Raman spectrum of n-type GaAs. The nominally undoped as-grown sample is dominated by the LO resonance (After Tiginyanu et al. 1997)

LO phonon resonance[1] (at 292 cm^{-1}) and some weak resonance of the forbidden TO phonon (at 268 cm^{-1}), while n-doped GaAs ($n = 3.5 \times 10^{17}$ cm^{-3}) shows the strong coupled plasmon modes ω_- and ω_+. Longitudinal plasmon modes can scatter with other quasi-particles such as LO phonons and electrons (Harper et al. 1973). The frequency of these plasmons increases with the square root of the electron density according to Eq. 4 and is on the order of the optical phonon frequencies at a carrier density between 10^{15} and 10^{17} cm^{-3}. Resonance effects occur which are similar to those of the photon – TO-phonon interaction leading to polaritons. However, the completely longitudinal plasma oscillation cannot interact with *transverse* electromagnetic radiation, leaving the TO phonon unaffected.

The occurrence of *two* Plasmon modes (Fig. 2a) originates from the photon-phonon interaction and a resulting typical split of the dispersion relation (shown in Fig. 2b) according to the von Neumann noncrosing rule, similar to the phonon-polariton discussed in ▶ Sect. 3.1 of chapter "Photon–Phonon Interaction". At low carrier density, the plasmon energy shows the square-root dependence on the carrier

[1]In optical spectroscopy energies are often given in units of cm^{-1}, which are related to eV units by 10 cm^{-1} ≅ 1.24 meV.

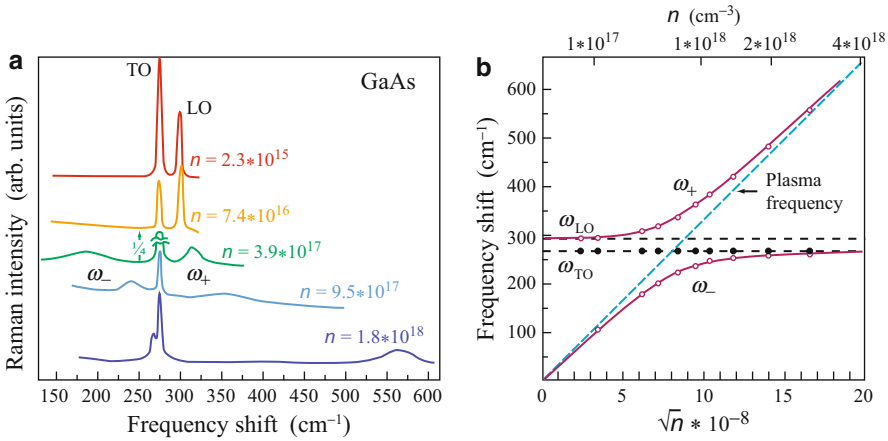

Fig. 2 (**a**) Anti-Stokes Raman scattering from plasmons coupled with LO phonons in *n*-type GaAs. The high-energy peak ω_+ shifts to higher energies, while the lower-energy peak ω_- approaches the TO peak with increasing electron density *n*. The TO peak remains at the same energy (After Mooradian and Wright 1966). (**b**) Eigenenergies of the mixed plasmon-phonon state in GaAs samples of different electron densities *n*; the TO phonon is unaffected (After Mooradian and McWhorter 1967)

density *n* according to Eq. 4. As the plasmon energy approaches the energy of LO phonons at higher carrier concentration, a mixed plasmon-phonon state is formed with two branches such that the dispersion curves of phonons and plasmon do not cross, see Fig. 2b.

This set of dispersion curves can be obtained from the polariton equation (Eq. 68 in chapter ▶ "Photon–Phonon Interaction"), considering plasmons instead. The LO resonance splits into two branches $\hbar\omega_+$ and $\hbar\omega_-$, given by

$$\omega_{\pm}^2 = \frac{1}{2}\left(\omega_{\mathrm{LO}}^2 + \omega_{\mathrm{p}}^2\right) \pm \frac{1}{2}\sqrt{\left(\omega_{\mathrm{LO}}^2 + \omega_{\mathrm{p}}^2\right)^2 - 4\omega_{\mathrm{p}}^2\omega_{\mathrm{TO}}^2} \tag{6}$$

and shown in Fig. 2b. The coupled mode energies can be obtained from the Raman spectra shown in Fig. 2a. The dots show the unchanged TO branch, and the circles show the two measured branches of the LO phonon as a function of the electron density, which causes the change of the plasmon frequency. The multiparticle interaction involves a phonon, a photon, and a plasmon (Patel and Slusher 1968). For more information, see Platzman and Wolff (1973).

The dielectric function of the plasmon follows from the oscillatory solution of Eq. 3; the oscillation amplitude is similar to Eq. 37 in chapter ▶ "Photon–Phonon Interaction",

$$\Delta x = \frac{eE_x}{m_n} \quad \frac{1}{\omega_{\mathrm{p}}^2 - \omega^2 - i\gamma\omega}. \tag{7}$$

For $\omega = \omega_p$ the amplitude is resonant and inverse to the damping parameter. This amplitude can be related to the polarization by

$$P_x = \frac{ne}{\varepsilon_{opt}} \Delta x. \tag{8}$$

From Eqs. 7 and 8, and Eq. 39 in chapter ▶ "Photon–Phonon Interaction" with Eq. 4, we obtain for the complex dielectric constant

$$\tilde{\varepsilon}(\omega) = \varepsilon' + i\varepsilon'' = \varepsilon_{opt} + \frac{\omega_p^2}{\omega_p^2 - \omega^2 - i\gamma\omega} \tag{9}$$

which can be separated into real and imaginary parts as

$$\varepsilon' = \varepsilon_{opt} + \omega_p^2 \left(\frac{\left(\omega_p^2 - \omega^2\right)}{\left(\omega_p^2 - \omega^2\right)^2 + \gamma^2\omega^2} \right) \tag{10}$$

and

$$\varepsilon'' = \omega_p^2 \frac{\omega\gamma}{\left(\omega_p^2 - \omega^2\right)^2 + \gamma^2\omega^2}. \tag{11}$$

Equations 10 and 11 have a form similar to Eqs. 44 and 45 in chapter ▶ "Photon–Phonon Interaction", except that the resonance frequency is given by the plasma frequency ω_p.

1.2 Valence-Electron Plasma Absorption

The plasmon absorption discussed before is caused by free electrons in the conduction band. In addition, we observe *valence-electron* plasmons when all the *valence*-electrons oscillate with respect to the cores. The mathematical theory is quite similar to that given in the previous section, except that in the expression for the plasmon frequency the density of *all* valence-electrons (typically 10^{23} cm^{-3}) is entered, m_n equals the electron rest mass, and the optical dielectric constant $\varepsilon \cong 1$. This results in a plasmon frequency of $\sim 10^{16}$ s^{-1} and a plasmon energy of ~ 10 eV.

The valence plasmon absorption can be measured as distinct losses when electrons penetrate through a thin layer of the semiconductor. The inelastic scattering of electrons is analyzed in electron energy-loss spectroscopy (EELS) typically carried out in a transmission-electron microscope; for a review see Egerton (2009). Figure 3 gives EELS spectra of GaN and $In_{0.5}Ga_{0.5}N$ regions in a nanowire, showing the composition dependence of the plasma peak within a selected small spot of 5–10 nm diameter. Typical plasmon energies are listed in Table 1.

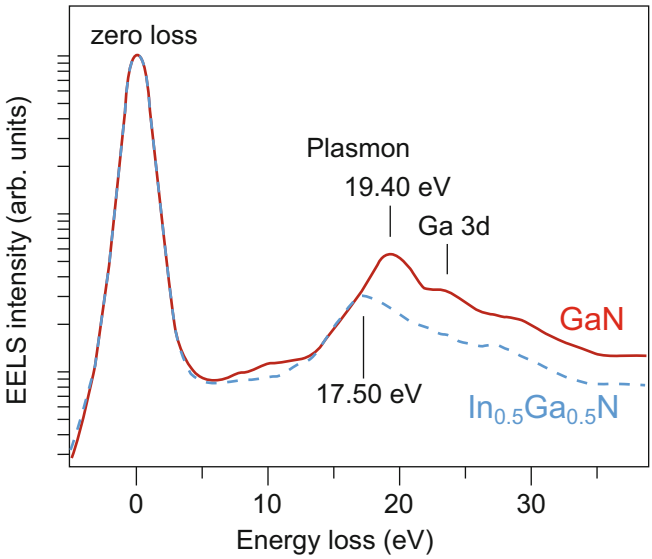

Fig. 3 Plasmon peaks in electron energy-loss spectra of GaN and $In_{0.5}Ga_{0.5}N$ (After Kong et al. 2012)

Table 1 Valence-electron plasmon energies of some semiconductors

Semiconductor	Si	Ge	GaP	GaAs	InP	InSb
$\hbar\omega_p$ (eV)	16.9	16.2	16.6	15.8	14.8	12.8

1.3 Charge-Density Waves

In materials with a high density of free electrons (metals or degenerate semiconductors) the conduction-electron charge-density, which is usually constant in a homogeneous material, can undergo a wave instability. Then the charge density becomes sinusoidally modulated in space (Overhauser 1978) with an extra periodicity not related to the lattice periodicity:

$$\rho(\mathbf{r}) = \rho_0(\mathbf{r})(1 + A\cos(\mathbf{qr} + \phi)), \tag{12}$$

where A is the amplitude (typically ~0.1 Å) and $\mathbf{q}$ is the wavevector of the charge-density wave

$$|\mathbf{q}| \cong 2p_F/\hbar \tag{13}$$

with p_F as the momentum at the (here assumed to be spherical) Fermi surface. In Eq. 12, ϕ is the phase. The charge-density wave is caused by the interaction between the electrons, which can be described by the exchange energy (Pauli principle) and the correlation energy (electron–electron scattering). Wave

formation tends to reduce these contributions. The Coulomb interaction counteracts the above-mentioned effects and suppresses wave formation. Additional interaction with the lattice cancels part of the suppression; hence in lattices with small elastic moduli, which could interact more readily, such charge-density waves are more likely to occur. Here, the lattice ions are also slightly displaced with an average amplitude of $\sim 0.01 \ldots 0.1$ Å and with the periodicity of the charge-density wave (Overhauser 1978). These waves are observed, e.g., in TaS_2 and $TaSe_2$, as two satellites to the Bragg reflection caused by the slight lattice displacement (Wilson et al. 1975).

A phase modulation, when quantized, can yield low-energy collective excitation spectra with quanta $\hbar\omega$ from

$$\phi = \phi(\mathbf{r}, t) \propto \sin(\mathbf{qr} - \omega t). \tag{14}$$

These are called *phasons* and are observed in $LaGe_2$. At low temperature, they could have a measurable effect on electron scattering (Huberman and Overhauser 1982).

2 Nonresonant Free-Carrier Absorption

Far away from the resonance transition at $\omega = \omega_p$, we observe the *nonresonant* part of the absorption with a much reduced amplitude, tailing from the resonance peak through the extrinsic optical absorption range and extending toward the band edge.

2.1 Dispersion Relation for Free Carriers

The optical absorption and reflection induced by free carriers outside of the resonance absorption provide valuable information about carrier relaxation and, for holes, about the band structure near $\mathbf{k} = 0$. The relationship between free carriers and an external field is the same as developed in Sect. 1.1 (Lax 1963), except that here the restoring forces are negligible and electrons respond only to external electromagnetic forces and damping:

$$m_n \left(\frac{d^2 \Delta x}{dt^2} - \gamma \frac{d\Delta x}{dt} \right) = -eE_x \exp(-i\omega t). \tag{15}$$

This equation of motion was introduced for the classical treatment of free-carrier dispersion (Drude model) by Drude (1900); it provides an independent opportunity to measure the electron scattering by optical absorption and will be discussed in more detail in the following section. The damping parameter γ can be related to the energy-relaxation time τ_{el} for a free electron by $\gamma = 1/\tau_{el}$. Equation 15 has the solution

$$\Delta x = -\frac{eE}{m_n} \quad \frac{1}{\omega^2 - i\omega/\tau_{\mathrm{el}}}. \tag{16}$$

The electric polarization P arising from bound *and* free electrons is then

$$P = \varepsilon_0\big(\varepsilon_{\mathrm{opt}} - 1\big)E + en\,\Delta x. \tag{17}$$

The complex dielectric function is related to P by $P = \varepsilon_0(\widetilde{\varepsilon} - 1)E$. Using this, we obtain from Eq. 17

$$\widetilde{\varepsilon}(\omega) = \varepsilon_{\mathrm{opt}}\left(1 - \frac{\omega_{\mathrm{p}}^2}{\omega^2 + i\omega/\tau_{\mathrm{el}}}\right), \tag{18}$$

where ω_{p} is given by Eq. 4. This dielectric function describes the response of free electrons on an external electromagnetic field. Equation 18 can be separated into real and imaginary parts as

$$\varepsilon' = n_{\mathrm{r}}^2 - \kappa^2 = \varepsilon_{\mathrm{opt}}\left(1 - \frac{\omega_{\mathrm{p}}^2}{\omega^2} \quad \frac{\omega^2\tau_{\mathrm{el}}^2}{1 + \omega^2\tau_{\mathrm{el}}^2}\right) \tag{19}$$

and

$$\varepsilon'' = 2n_{\mathrm{r}}\kappa = \varepsilon_{\mathrm{opt}}\frac{\omega_{\mathrm{p}}^2}{\omega^2} \quad \frac{\omega\tau_{\mathrm{el}}}{1 + \omega^2\tau_{\mathrm{el}}^2}. \tag{20}$$

Equations 19 and 20 have a form similar to the resonance case of Eqs. 44 and 45 in chapter ▶ "Photon–Phonon Interaction", except that the resonance frequency here is zero. Free carriers give a *negative* contribution to ε' and, hence, to the index of refraction n_{r}.

There is another approach to the free-carrier dielectric function and optical absorption. Is is used here for educational purposes in order to arrive directly at the complex conductivity (see ▶ Sect. 1.1.4 in chapter "Interaction of Light with Solids"):

$$\frac{d\Delta x}{dt} = v_x = -\frac{eE}{m_n}\frac{\tau_{\mathrm{el}}}{1 - i\omega\tau_{\mathrm{el}}}. \tag{21}$$

This velocity can be used to define an electric current density[2]

[2]This is an ac current at the frequency ω which, for higher ω (i.e., for $\omega \geq \tau_{\mathrm{el}}^{-1}$), is substantially different from the dc current, as indicated in ▶ Sect. 1.1.4. of chapter "Interaction of Light with Solids"

$$\tilde{j}_x = -e\,n\,\tilde{v}_x = \tilde{\sigma}\,E, \tag{22}$$

with a complex conductivity

$$\tilde{\sigma} = \sigma' + i\,\sigma'' = \sigma_0\left(\frac{1}{1+\omega^2\tau_{\mathrm{el}}^2} + i\,\frac{\omega\,\tau_{\mathrm{el}}}{1+\omega^2\tau_{\mathrm{el}}^2}\right), \tag{23}$$

with $\sigma_0 = e^2\,n\tau_{\mathrm{el}}/m_n$ as the dc conductivity. Introducing Eq. 23 into $\mathbf{j}(\omega)$ given in ▶ Eq. 26 of chapter "Interaction of Light with Solids", we obtain with $\sigma_0 = \omega_{\mathrm{p}}^2\tau_{\mathrm{el}}$ $\varepsilon_0\varepsilon_{\mathrm{opt}}$ again (Eqs. 19 and 20).

We can experimentally obtain ω_{p} and $\varepsilon_{\mathrm{opt}}$ by measuring the reflectance. In the frequency range where $n_{\mathrm{r}}^2 \gg \kappa^2$ we obtain from Eq. 54 in chapter ▶ "Interaction of Light with Solids"

$$R_0 \cong \frac{(n_{\mathrm{r}}-1)^2}{(n_{\mathrm{r}}+1)^2} \text{ or } n_{\mathrm{r}} \cong \frac{1+\sqrt{R_0}}{1-\sqrt{R_0}}. \tag{24}$$

The index of refraction as a function of ω for the condition $n_{\mathrm{r}}^2 \gg \kappa^2$ refers to $\omega\tau_{\mathrm{el}} \gg 1$, yielding from Eq. 19

$$n_{\mathrm{r}}^2 \cong \varepsilon_{\mathrm{opt}}\left(1 - \frac{\omega_{\mathrm{p}}^2}{\omega^2}\right) = \varepsilon_{\mathrm{opt}} - \frac{\lambda^2\ e^2}{4\pi^2\,c^2\varepsilon_0^2 m_n}. \tag{25}$$

In the last expression, we have used $\omega = 2\pi\,c/\lambda$. The frequencies $\omega_{\min}$ and $\omega_{\max}$ at which the reflection minimum and maximum occur are those for which $R_0 \ll 1$ (or $n_{\mathrm{r}} \cong 1$) and $R_0 \cong 1$ (or $n_{\mathrm{r}} \cong 0$), respectively; they are related to ω_{p} and $\varepsilon_{\mathrm{opt}}$ using Eq. 25 by

$$\omega_{\min} \cong \omega_{\mathrm{p}}\sqrt{\frac{\varepsilon_{\mathrm{opt}}}{\varepsilon_{\mathrm{opt}}-1}} \text{ and } \omega_{\max} \cong \omega_{\mathrm{p}}. \tag{26}$$

With known $\varepsilon_{\mathrm{opt}}$, we have a useful method for determining ω_{p}, and with it the effective carrier mass in ω_{p} (Eq. 4), provided the carrier density is known by independent means. We can vice versa extract the carrier density from reflection spectra if the effective mass is known. Typical IR reflection spectra observed for n-type InP are shown in Fig. 4, with reflection minima shifting to higher energies with increasing carrier density according to Eqs. 4 and 26.

To conclude, when the concentration of free carriers is sufficiently high, the reflection in the IR range between the wavelength corresponding to the bandgap and the Reststrahlen wavelength is strongly influenced by free carriers. From an analysis of the reflection spectra, we can obtain the plasma frequency. For a review of optical characterization of free carriers in semiconductors see Palik and Holm (1979).

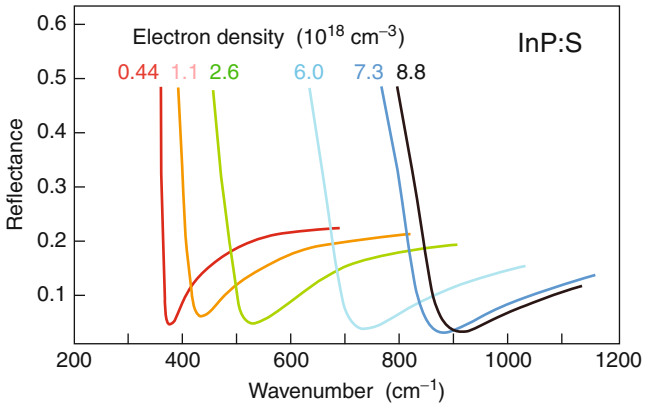

Fig. 4 Infrared reflectance of *n*-type InP with various doping densities (After Kim and Bonner 1983)

2.2 Free-Electron Absorption

The optical absorption coefficient due to free electrons is obtained from Eq. 24 in chapter ▶ "Interaction of Light with Solids" and Eq. 20:

$$\alpha_o = \frac{2\omega\kappa}{c} = \frac{\omega}{c}\frac{\varepsilon''}{n_r} = \frac{\omega_p^2}{n_r\ c}\ \frac{\tau_{el}}{1+\omega^2\tau_{el}^2}. \tag{27}$$

The strength of the absorption is $\propto \omega_p^2$. For high enough frequencies ($\omega\tau_{el} \gg 1$), Eq. 27 becomes the classical $\alpha_o \propto \lambda^2$ relation

$$\alpha_o = \frac{\omega_p^2}{\omega^2}\ \frac{1}{n_r c\tau_{el}} = \frac{\omega_p^2\lambda^2}{4\pi^2 n_r c^3\tau_{el}}. \tag{28}$$

$$= 3\times 10^{-4}\frac{10}{\varepsilon_{opt}}\ \frac{m_0}{m_n}\ \frac{n}{10^{16}(\mathrm{cm}^{-3})}\ \frac{\lambda^2(\mu\mathrm{m})^2}{n_r}\ \frac{10^{-13}\mathrm{s}}{\tau_{el}}$$

Such behavior is often observed for the free-electron absorption in the extrinsic range beyond the band edge. The free-electron absorption is a continuous absorption tailing off from the lattice resonances toward the band edge (Fig. 5). This absorption is rather small near the absorption edge for semiconductors with normal electron densities and becomes observable in the IR only at higher levels of doping ($n > 10^{17}$ cm^{-3} – see Fig. 5a) when the probing frequency is closer to the plasma frequency – see Sect. 1.1.

In the following section, we will show that this λ^2 relation is modified by specific scattering mechanisms of the carriers when this scattering depends on the energy of the carrier within the band; here $\tau_{el} = \tau_{el}(\lambda)$, and α_o becomes a more complicated function of λ.

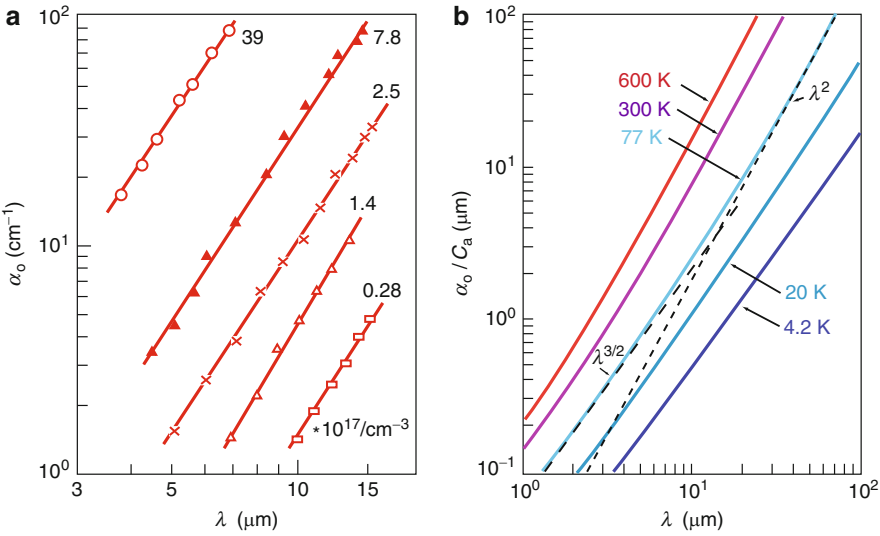

Fig. 5 (**a**) Optical absorption of free electrons with predominant acoustic phonon scattering beyond the band edge of *n*-type InAs at room temperature for various electron densities (After Dixon 1960). (**b**) Optical absorption of free electrons as in (**a**), at various temperatures, with C_a (μm^2) a proportionality factor (After Seeger 1973)

2.2.1 Effect of Scattering Mechanisms on Free-Electron Absorption

Examining the electronic band structure $E(\mathbf{k})$ of a typical conduction bands, we recognize that direct optical transitions of electrons in the conduction bands, which are essentially vertical in $E(\mathbf{k})$, are rather rare events. They are restricted to transitions at specific values of $\mathbf{k}$, which find an allowed $E(\mathbf{k})$ for the given photon energy (e.g., $h\nu_{dir}(3)$ in Fig. 6) *and* a sufficiently large occupation probability of the ground state from which such a transition (3) starts. Only from the minimum of the conduction band to a band above it are such transitions plentiful (at the Γ-point with $h\nu_{dir}$ (1) in Fig. 6). For most other photon energies, only indirect transitions are possible – see ▶ Sect. 2 in chapter "Band-to-Band Transitions". They require the supply or emission of a phonon in addition to the absorption of the photon, as shown in Fig. 6 as transition $h\nu_{indir}(2) = h\nu_{dir}(2) \pm \hbar\omega_p$.

The transition probability for such indirect transitions can be calculated from a second-order perturbation theory (see Sakurai and Napolitano 2011) including the Hamiltonian for a photon and the Hamiltonian for a phonon transition. This is necessitated by the fact that three particles are involved in the transition: a photon, an electron, and a phonon or a lattice defect. The interaction is much like that of the scattering of an electron with a phonon: the electron is first elevated by the photon to a virtual state within the conduction band.

The mathematical formulation of the theory for the scattering with different types of phonons is similar to the analysis of the electron scattering for carrier transport (chapter ▶ "Carrier Scattering at Low Electric Fields") or for

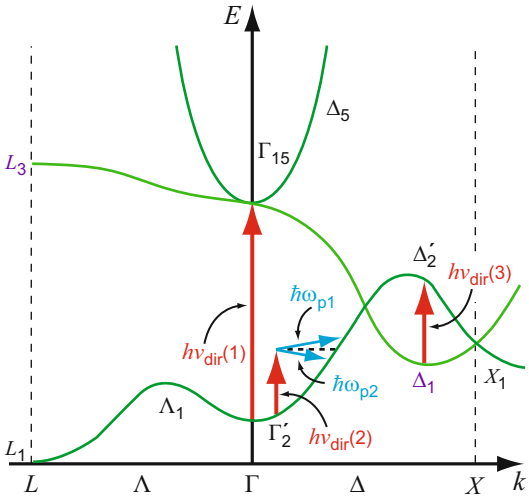

Fig. 6 Direct ($h\nu_{\mathrm{dir}}$) and indirect transitions ($h\nu_{\mathrm{indir}} = h\nu_{\mathrm{dir}} \pm \hbar\omega_{\mathrm{p}}$) for free electrons within conduction bands. The indirect transition requires, in addition to the absorption of a photon $h\nu_{\mathrm{dir}}$, the absorption ($\hbar\omega_{\mathrm{p1}}$) or emission ($\hbar\omega_{\mathrm{p2}}$) of a phonon of the proper energy and momentum

higher energies within the band (chapter ▶ "Carrier Scattering at High Electric Fields" – see also Seeger 2004). In a first approximation, the optical absorption coefficient can be expressed by the classical free-electron absorption α_{o} Eq. 28 and by replacing the electron relaxation time τ_{el} with the one relating to the predominant scattering mechanism. This permits the replacement of the yet unknown τ_{el} in Eq. 28 with an appropriate expression (see Seeger 2004).

For instance, we obtain for predominant *acoustic deformation potential scattering* with a phonon energy being much smaller than the photon energy $\hbar\omega_q \ll h\nu$:

$$\alpha_{\mathrm{o,ac},E} \cong \alpha_{\mathrm{o,ac}} \frac{h\nu}{4\ kT} \sqrt{\frac{T}{T_{\mathrm{el}}}} \sinh\left(\frac{h\nu}{2\ kT_{\mathrm{el}}}\right) K_2\left(\frac{h\nu}{2\ kT_{\mathrm{el}}}\right), \tag{29}$$

where T_{el} is the electron temperature[3] and $h\nu$ is the energy of the absorbed photon; K_2 is a modified Bessel function (Poole 1998).

When only small deviations from thermal equilibrium are considered ($T_{\mathrm{el}} \cong T$) and the photon energy is small compared to the thermal energy ($h\nu \ll kT$), then the factor following $\alpha_{\mathrm{o,ac}}$ approaches 1 and $\alpha_{\mathrm{o,ac},E} \cong \alpha_{\mathrm{o,ac}}$ with

$$\alpha_{\mathrm{o,ac}} = \alpha_{\mathrm{o}} \frac{2^{7/2}(m_n kT)^{3/2} \Xi_{\mathrm{c}}^2}{3\pi^{3/2}\hbar^4 C_l} \tag{30}$$

and α_{o} given by Eq. 28. Here Ξ_{c} is the deformation potential for the conduction band, and C_l is the appropriate elastic stiffness constant. Also, $\alpha_{\mathrm{o,ac}}$ shows the classical λ^2 behavior (contained in α_{o}) as indicated in Fig. 5a.

[3] An elevated (above the lattice temperature) electron temperature is used here to indicate the occupancy of states higher in the conduction band by electrons.

For photons with higher energies (for $h\nu \gg kT$), however, one obtains

$$\alpha_{o,\,ac,\,E} \cong \frac{\alpha_{o,\,ac}}{2}\sqrt{\frac{\pi}{2}\frac{h\nu}{kT}} \propto \lambda^{3/2}, \tag{31}$$

which gives a somewhat lower slope (when the emission of many phonons becomes possible), which is indicated in Fig. 5b.

There are substantial differences for the scattering of electrons which are excited into higher band states. From here, scattering is greatly enhanced by rapid generation of LO phonons (▶ Sect. 3 in chapter "Carrier Scattering at High Electric Fields"). This scattering can be described as the scattering of a *heated electron gas* with T_{el} much larger than T.

The absorption coefficients for other phonon-scattering mechanisms show a wavelength dependence similar to the acoustic one for long-wavelength excitation. However, at low temperatures, it becomes nonmonotonic as soon as the electron energy exceeds that of the rapidly generated optical phonons (Fig. 7a). At low temperature LO phonons are frozen-out; a low scattering and therefore a low absorption results. When the electrons gain energy above $\hbar\omega_{LO}$ with decreasing λ of the exciting light, the relaxation time decreases dramatically, and therefore

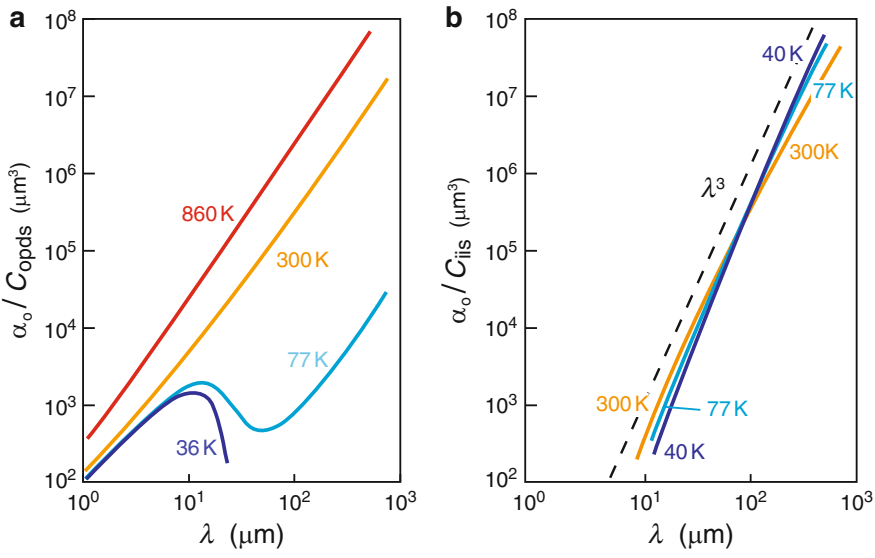

Fig. 7 (**a**) Optical absorption of free electrons computed for predominant optical deformation potential scattering with $\Theta = 720$ K and C_{opds} a proportionality factor of dimension cm^{-2} at various temperatures. (**b**) Optical absorption of free electrons computed for ionized impurity scattering with C_{iis} a proportionality factor of dimension cm^{-2} at various temperatures (After Seeger 1973)

$\alpha_{o,opt,E}$ increases. At high temperatures this resonance is hidden since there are enough electrons thermally excited near $\hbar\omega_{LO}$.

The maximum is due to resonance scattering when the electron energy within the band equals that of the LO phonon. This nonmonotonic behavior is observed for *optical deformation potential scattering* as well as for *polar optical scattering,* for which the wavelength dependence increases from λ^2 to $\lambda^{2.5}$ for higher energies.

For lower temperatures ($kT < \hbar\omega_{LO}/2$) near thermal equilibrium ($T_{el} = T$) one obtains for the ratio of optical and acoustic deformation potential scatterings:

$$\frac{\alpha_{o,\,opt}}{\alpha_{o,\,ac}} = \frac{4}{\sqrt{\pi}}\left(\frac{D_o v_l}{\Xi_c \omega_0}\right)^2 \sqrt{\frac{t}{\Theta}}, \tag{32}$$

where D_o and Ξ_c are the optical and acoustic deformation potential constants, and v_l is the longitudinal sound velocity. Here Θ is the Debye temperature.

Ionized impurity scattering (Wolfe 1954) causes a stronger dependence on the wavelength, which for higher energies approaches λ^3:

$$\alpha_{o,\,ion} \propto \frac{N_{ion} Z_{ion} e^4}{3\sqrt{2}\pi^{3/2}(\varepsilon\varepsilon_0)^2 (mkT_{el})^{1/2} h\nu} \sinh\left(\frac{h\nu}{2\ kT_{el}}\right) K_0\left(\frac{h\nu}{2\ kT_{el}}\right) \propto \lambda^3, \tag{33}$$

where K_0 is a modified Bessel function (Poole 1998). The computed absorption behavior for scattered ionized impurities is shown in Fig. 7b.

With different scattering mechanisms, the optical absorption coefficients for each one of them is added (the inverse of the relaxation times are added – see Eq. 28) in order to obtain the total optical absorption:

$$\alpha_{o,\,total} = \sum_i \alpha_{o,i}. \tag{34}$$

When studying a family of absorption curves at different temperatures, we can obtain some information about the predominant scattering mechanism, especially about scattering at higher electron energies for semiconductors with sufficient electron densities.

2.2.2 Free-Hole Absorption

The absorptions of free electrons and holes follow similar principles. However, although most electron transitions within the conduction band are indirect, requiring the emission or absorption of phonons (Fan 1967), the most prevalent long-wavelength transitions for holes are direct, as shown in Fig. 8. Therefore, under otherwise similar conditions, the absorption coefficient for holes is much larger than that for electrons.

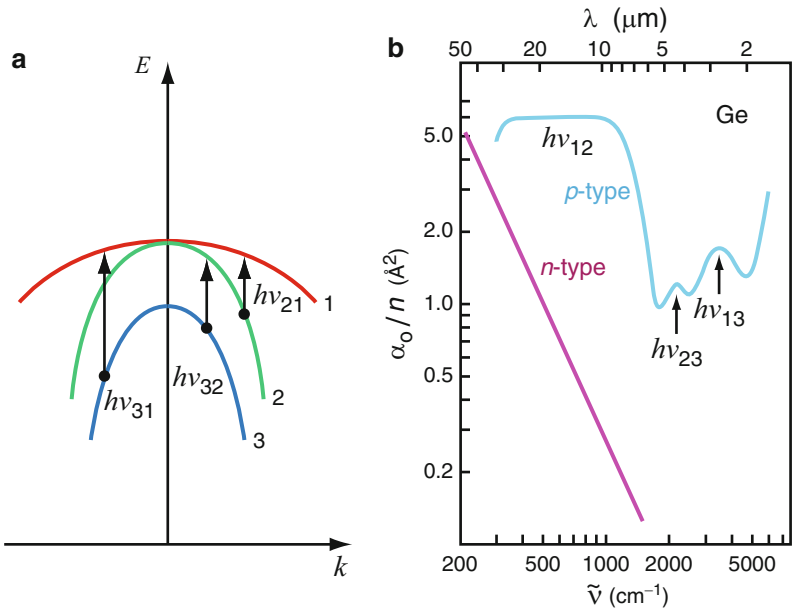

Fig. 8 (**a**) Schematic of intervalence-band transitions. (**b**) Optical absorption cross-section as a function of wavelength (wavenumbers) for *n*- and *p*-type Ge (After Kaiser et al. 1953)

Closely spaced valence bands (Fig. 8a) provide possibilities for a wide spectrum of direct transitions at very long wavelengths. In addition, the change from heavy to light holes, detected by simultaneous conductivity measurements, assists in identifying the specific feature in the absorption spectrum.

Steps in the optical absorption spectrum are observed when the energy of the holes is sufficient to permit optical phonon relaxation. Such a step was calculated for a single threshold in the electron energy for $\hbar\omega_{\mathrm{LO}}$ emission (see section above and Fig. 7a).

3 Carrier Dispersion in Electric and Magnetic Fields

The dispersion equation with an additional magnetic field is obtained from Maxwell's equations, exactly as in ▶ Sect. 1.1.3 from Eq. 17 in chapter "Interaction of Light with Solids", except that the magnetic field causes a change in wave propagation or polarization and therefore requires a vector relation for the amplitude function $\mathbf{E}(x)$, resulting in

$$\frac{\partial^2}{\partial \mathbf{r}^2}\mathbf{E} + \frac{\omega^2}{c^2}\left(\underline{\boldsymbol{\varepsilon}} + \frac{i}{\varepsilon_0\,\omega}\underline{\boldsymbol{\sigma}}(\mathbf{B})\right)\ \mathbf{E} = 0. \tag{35}$$

where $\underline{\boldsymbol{\varepsilon}}$ and $\underline{\boldsymbol{\sigma}}$ are the *dielectric* and the *conductivity matrices*, respectively. The dielectric matrix is not influenced by the magnetic field. For isotropic crystals, we can simply use the dielectric constant, requiring, however, matrix notation to permit matrix calculus. For a magnetic induction in the z direction, the $\underline{\boldsymbol{\sigma}}$ matrix simplifies to

$$\underline{\boldsymbol{\sigma}} = \begin{pmatrix} \sigma_{xx} & \sigma_{xy} & \\ \sigma_{yx} & \sigma_{yy} & \\ & & \sigma_{zz} \end{pmatrix}. \tag{36}$$

The components of this matrix are obtained from the equation of motion, which is identical to Eq. 15, except for the addition of the Lorentz force $e(\mathbf{v}_{\text{drift}} \times \mathbf{B})$:

$$m_n \left(\frac{d\mathbf{v}_{\text{drift}}}{dt} + \frac{\mathbf{v}_{\text{drift}}}{\tau_{\text{mag}}} \right) = e(\mathbf{E} + \mathbf{v}_{\text{drift}} \times \mathbf{B}). \tag{37}$$

We assume an isotropic effective mass m_n and an isotropic relaxation time τ_{mag} independent on the velocity. With $\mathbf{E} = \mathbf{E}(x)\exp(-i\omega t)$ and $en\mathbf{v}_{\text{drift}} = \underline{\boldsymbol{\sigma}}(B)\mathbf{E}$, we obtain

$$\sigma_{xx} = \sigma_{yy} = \sigma_0 \frac{1 - i\omega\tau_{\text{mag}}}{\left(1 - i\omega\tau_{\text{mag}}\right)^2 + \left(\omega_{\text{c}}\,\tau_{\text{mag}}\right)^2} \tag{38}$$

$$\sigma_{xy} = -\sigma_{yx} = \sigma_0 \frac{\omega_{\text{c}}\,\tau_{\text{mag}}}{\left(1 - i\omega\tau_{\text{mag}}\right)^2 + \left(\omega_{\text{c}}\,\tau_{\text{mag}}\right)^2} \tag{39}$$

$$\sigma_{zz} = \sigma_0 \frac{1}{1 - i\omega\tau_{\text{mag}}}, \tag{40}$$

with $\omega_{\text{c}} = eB/m_n$ as the cyclotron frequency and $\sigma_0 = e^2 n\tau_{\text{mag}}/m_n = en\mu$ as the dc conductivity. Given the magnetic induction $\mathbf{B} = (0, 0, B_z)$, we can distinguish from the general dispersion equation[4]

$$k^2\mathbf{E} = \frac{\omega^2}{c^2}\underline{\boldsymbol{\varepsilon}}\mathbf{E} + i\frac{\omega}{\varepsilon_0\, c^2}\underline{\boldsymbol{\sigma}}(B)\mathbf{E}, \tag{41}$$

a number of cases depending on the relative orientation of the propagation ($\mathbf{k}$) and polarization ($\mathbf{E}$) of the light interacting with the semiconductor. These cases are identified in Table 2.

[4]Obtained from Eq. 35 with $\mathbf{E} = \mathbf{E}_0\exp[i(\mathbf{k}\mathbf{r} - \omega t)]$.

Table 2 Various cases for dispersion relations discussed in the text, depending on the relative orientation of **B**, **k**, and **E**

Magnetic induction	$\mathbf{B} = (0, 0, B_z)$	
Wave propagation	Longitudinal Faraday configuration $\mathbf{k} = (0, 0, k_z)$	Transverse Voigt configuration $\mathbf{k} = (0, k_y, 0)$
Electric vector linear Linear Circular	$\mathbf{E} = (0, E_y, 0)$ $\mathbf{E} = (E_x, 0, 0)$ $\mathbf{E} = (E_x \pm i\,E_y)$	$\mathbf{E} = (0, 0, E_z)$ $\mathbf{E} = (E_x, 0, 0)$

For the *longitudinal case* one has

$$k_z^2 E_x = \frac{\omega^2}{c^2}\varepsilon_{\text{opt}} E_x + i\frac{\omega}{\varepsilon_0 c^2}\left(\sigma_{xx}E_x + \sigma_{xy}E_y\right). \tag{42}$$

$$k_z^2 E_y = \frac{\omega^2}{c^2}\varepsilon_{\text{opt}} E_y + i\frac{\omega}{\varepsilon_0 c^2}\left(-\sigma_{xy}E_x + \sigma_{xx}E_y\right). \tag{43}$$

For *circular polarizarized light* ($E_x \pm i\,E_y$) we obtain by using $k_z^2(\omega/c)^2(n + i\kappa)^2$ and adding Eq. 42 $\pm\, i \times$ Eq. 43

$$(n_\pm + i\kappa_\pm)^2 = \varepsilon_{\text{opt}} + i\frac{\sigma_\mp}{\varepsilon_0\,\omega} \quad \text{with} \quad \sigma_\mp = \sigma_{xx} \mp i\sigma_{xy}. \tag{44}$$

After separation of real and imaginary parts we arrive at

$$\varepsilon'_\pm = \left(n_\pm^2 - \kappa_\pm^2\right) = \varepsilon_{\text{opt}}\left(1 - \frac{\omega_\text{p}^2\,\tau_{\text{mag}}^2}{\omega}\,\frac{\omega \pm \omega_\text{c}}{\left[(\omega \pm \omega_\text{c})\;\tau_{\text{mag}}\right]^2 + 1}\right) \tag{45}$$

$$\varepsilon''_\pm = 2n_\pm\kappa_\pm = \varepsilon_{\text{opt}}\left(1 - \frac{1}{\omega}\,\frac{\omega_\text{p}^2\,\tau_{\text{mag}}}{\left[(\omega \pm \omega_\text{c})\;\tau_{\text{mag}}\right]^2 + 1}\right). \tag{46}$$

with the + or – sign for right- or left-polarized light, respectively, and ω_p the plasma frequency (Eq. 4).

For the *transverse case* there are three dispersion equations:

$$k_y^2 E_x = \frac{\omega^2}{c^2}\varepsilon_{\text{opt}} E_x + i\frac{\omega}{\varepsilon_0 c^2}\left(\sigma_{xx}E_x + \sigma_{xy}E_y\right), \tag{47}$$

$$0 = \frac{\omega^2}{c^2}\varepsilon_{\text{opt}} E_y + i\frac{\omega}{\varepsilon_0 c^2}\left(-\sigma_{xy}E_x + \sigma_{xy}E_y\right), \tag{48}$$

$$k_y^2 E_z = \frac{\omega^2}{c^2}\varepsilon_{\text{opt}} E_z + i\frac{\omega}{\varepsilon_0 c^2}\sigma_{zz}E_z, \tag{49}$$

which yield for *parallel polarization* (**E**||**B**)

$$\widetilde{\varepsilon}_{||}\left(n_{||}+i\kappa_{||}\right)^2=\varepsilon_{\text{opt}}+i\frac{\sigma_{zz}}{\varepsilon_0\,\omega}, \tag{50}$$

with

$$\varepsilon'=\varepsilon_{\text{opt}}\left(1-\frac{\left(\omega_{\text{p}}\,\tau_{\text{mag}}\right)^2}{\left(\omega\,\tau_{\text{mag}}\right)^2+1}\right)\text{and}\,\varepsilon''=\varepsilon_{\text{opt}}\frac{1}{\omega}\,\frac{\omega_{\text{p}}^2\,\tau_{\text{mag}}}{\left(\omega\,\tau_{\text{mag}}\right)^2+1}. \tag{51}$$

For the *perpendicular polarization* (**E**⊥**B**) we have

$$\widetilde{\varepsilon}_{\perp}(n_{\perp}+i\kappa_{\perp})^2=\varepsilon_{\text{opt}}+i\frac{1}{\varepsilon_0\,\omega}\left(\sigma_{xx}+i\frac{\sigma_{xy}^2}{\varepsilon_{\text{opt}}\varepsilon_0\omega+i\sigma_{xx}}\right) \tag{52}$$

with

$$\varepsilon'=\varepsilon_{\text{opt}}\left(1-\frac{\left(\omega_{\text{p}}\,\tau_{\text{mag}}\right)^2\ \beta}{\left(\omega\,\tau_{\text{mag}}\right)^2\beta^2+\alpha^2}\right)\text{and}\ \varepsilon''=\varepsilon_{\text{opt}}\frac{1}{\omega}\,\frac{\omega_{\text{p}}^2\,\tau_{\text{mag}}\,\alpha}{\left(\omega\,\tau_{\text{mag}}\right)^2\beta^2+\alpha^2} \tag{53}$$

and with the auxiliary functions

$$\alpha=1+\frac{\omega^2\,\tau_{\text{mag}}^2\omega_{\text{c}}^2}{\omega^2+\left[\left(\omega^2-\omega_{\text{p}}^2\right)\ \tau_{\text{mag}}\right]^2}\ \text{and}\ \beta=1-\frac{\left(\omega^2-\omega_{\text{p}}^2\right)\tau_{\text{mag}}^2\omega_{\text{c}}^2}{\omega^2+\left[\left(\omega^2-\omega_{\text{p}}^2\right)\ \tau_{\text{mag}}\right]^2}. \tag{54}$$

There are two characteristic frequencies entering the dispersion equation: the plasma (ω_{p}) and the cyclotron (ω_{c}) frequencies, which determine possible resonances. The damping is determined by the appropriate relaxation time and gives the width of the resonance peak. These equations describe all possible interactions of electromagnetic radiation with a semiconductor while exposed to a dc magnetic induction. Examples for such interactions are cyclotron resonance, magnetoplasma reflection, and the Faraday and Voigt effects. They will be discussed in the following sections. For more detail, see Madelung (1978), Roth (1982), Basu (1997), and Sugano and Kojima (2000).

3.1 Magnetoplasma Reflection

A relatively simple means to determine one or both of the characteristic frequencies ω_{c} and ω_{p} – and thereby the effective mass, carrier type, and carrier density – is to measure the spectral distribution of the reflectivity with **k**||**B** or **k**⊥**B**, i.e., for

Faraday or Voigt configuration, respectively. The effect in reflectivity can be derived by substituting the magneto-optical constants $n_{\pm}$, $\kappa_{\pm}$, $n_{\|}$, $n_{\perp}$, $\kappa_{\|}$, and $\kappa_{\perp}$ in the Fresnel formula for the reflection coefficient (Eq. 54 in chapter ▶ "Interaction of Light with Solids"):

$$R_0 = R_{\perp} = R_{\|} = \frac{(n_r - 1)^2 + \kappa^2}{(n_r + 1)^2 + \kappa^2}. \tag{55}$$

Faraday Configuration Arranging the propagation of the interacting light parallel to the magnetic induction and using circular polarized light yields a reflectivity

$$R_{\pm} = \frac{(n_{\pm} - 1)^2 + \kappa_{\pm}^2}{(n_{\pm} + 1)^2 + \kappa_{\pm}^2}. \tag{56}$$

For $n_{+}^2 \gg \kappa_{-}^2$, the reflectivity shows a maximum (see Eq. 45) when the index of refraction tends to vanish ($n_{\pm} \cong 0$) – that is, when

$$\omega \cong \omega_p \pm \frac{1}{2}\omega_c + \frac{\sqrt{\varepsilon_{opt}}}{8}\frac{\omega_c^2}{\omega_p} \tag{57}$$

for left (−) or right (+) circular polarized light. Consequently, a shift in the plasma edge by $\pm\,\omega_c/2$ is seen (when $\omega_p \gg \omega_c$) when a magnetic induction is applied. This is shown in Fig. 9a for InSb and can be used to determine ω_c and thereby the effective mass.

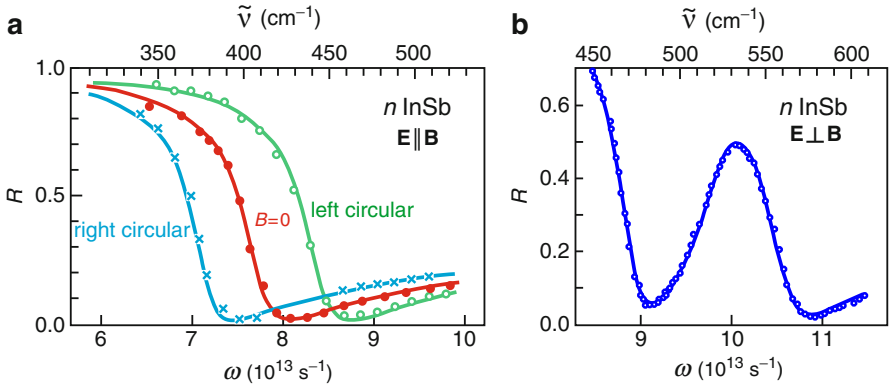

Fig. 9 (**a**) Shift of the plasma absorption edge in *n*-type InSb at room temperature for $n = 10^{18}$ cm^{-3}, $\tau_{el} = 2.8 \cdot 10^{-13}$s, and $m_n/m_0 = 0.035$ at $\mathbf{B} = 0$ and ±2.54 T (Faraday configuration); the curves are calculated (After Palik et al. 1962). (**b**) Transverse magnetoplasma reflection (Voigt configuration) in *n*-type InSb at room temperature for $n = 1.8 \cdot 10^{18}$ cm^{-3}, $\tau_{el} = 3.6 \cdot 10^{-13}$s, and $B = 3.52$ T (After Wright and Lax 1961)

Voigt Configuration With plane-polarized light at normal incidence to the crystal surface and the magnetic vector parallel to the surface, we obtain for $\mathbf{E}\perp\mathbf{B}$ as a condition for minimum reflection ($R_\perp \cong 0$ because of $n_\perp \to 1$) from Eq. 53, neglecting the damping term:

$$\omega^4\left(\frac{\varepsilon_{\text{opt}}-1}{\varepsilon_{\text{opt}}}\right)-\omega^2\left[\left(\frac{\varepsilon_{\text{opt}}-1}{\varepsilon_{\text{opt}}}\right)\left(\omega_{\text{p}}^2+\omega_{\text{c}}^2\right)+\omega_{\text{p}}^2\right]+\omega^4=0 \tag{58}$$

which has two minima at

$$\omega_1^2\cong\omega_{\text{p}}^2\left(\frac{\varepsilon_{\text{opt}}}{\varepsilon_{\text{opt}}-1}\right)+\varepsilon_{\text{opt}}\,\omega_{\text{c}}^2 \quad\text{and}\quad \omega_2^2\cong\omega_{\text{p}}^2-\omega_{\text{c}}^2\left(\varepsilon_{\text{opt}}-1\right). \tag{59}$$

They are shown in Fig. 9b for n-type InSb from which the cyclotron frequency, and thereby the effective mass, can be obtained. Once the cyclotron frequency is known, the plasma frequency can also be obtained and thereby the carrier density. For more information on magneto-optical and magnetoplasma effects, see Palik and Wright (1967), Maan (1993), and Seeger (2004).

3.2 Cyclotron-Resonance Absorption and Faraday Effect

3.2.1 Cyclotron-Resonance Absorption

Cyclotron-resonance absorption occurs when the frequency of the impinging electromagnetic radiation (usually in the microwave range) equals the cyclotron frequency (eB/m_n). It is measured with $\mathbf{k}\|\mathbf{B}$ and linear polarized $\mathbf{E} = (E_x, 0, 0)$ radiation, which renders (Eq. 42)

$$k_z^2=\frac{\omega^2}{c^2}\,\varepsilon_{\text{opt}}+i\frac{\omega}{\varepsilon_0\,c^2}\,\sigma_{xx}. \tag{60}$$

With $k_z^2=(\omega/c)^2\,\tilde{n}_{\text{r}}^2=(\omega/c)^2(n_{\text{r}}+i\kappa)^2$ we obtain with (Eq. 38)

$$2n_{\text{r}}\kappa=\frac{1}{\varepsilon_0\,\omega}\,\sigma_{xx}=\frac{\sigma_0}{\varepsilon_0\,\omega}\,\frac{1+\left(\omega_{\text{c}}^2+\omega^2\right)\tau_{\text{mag}}^2}{\left[1+\left(\omega_{\text{c}}^2-\omega^2\right)\,\tau_{\text{mag}}^2\right]^2+4\omega^2\,\tau_{\text{mag}}^2}. \tag{61}$$

Cyclotron resonance effectively determines ω_{c}, which is a direct measure of the effective mass. By rotating the semiconductor with respect to $\mathbf{B}$, one obtains m_n as a function of the crystallographic orientation. This was discussed in more general terms in ▶ Sect. 1.2.5 of chapter "Bands and Bandgaps in Solids".

In addition to the conventional method of observing cyclotron resonance by microwave absorption, one can detect the resonances optically by exciting carriers near the band edges. With a magnetic field applied, electrons are forced into orbits

with the cyclotron frequency ω_c and the band states split into Landau levels with spacing $\hbar\omega_c$. The ensuing mixed collective mode frequency in Voigt configuration is then composed of three frequencies,

$$\omega_{\pm} = \frac{1}{2}\left(\omega_p^2 + \omega_c^2 + \omega_{LO}^2\right) \pm \frac{1}{2}\sqrt{\left(\omega_p^2 + \omega_c^2 + \omega_{LO}^2\right)^2 - 4\left(\omega_c^2\omega_{LO}^2 + \omega_p^2\omega_{LO}^2\right)}. \tag{62}$$

Consequently, the resonances become magnetic field dependent. These resonances are given by $\omega_c^2 + \omega_p^2 = \omega_{LO}^2$ (Palik and Furdyna 1970). In Faraday configuration, strong absorption occurs at $\omega = \omega_c$ or $\omega = \omega_{TO}$, the former is independent of lattice coupling. In addition to the resonant Raman scattering at ω_c, two-photon resonances occur when $\omega_1 - \omega_2 = 2\omega_c$ (Patel and Slusher 1968).

In *superlattices*, the confinement of cycling electrons within each well can be easily detected by the optical method described before (Cavenett and Pakulis 1985): the resonances become angle-dependent and are pronounced only within the plane of the superlattice, where electrons can follow the Lorentz force.

3.2.2 Faraday Effect

The dispersion relation for circular polarized light (Eqs. 44 to 46) with $\mathbf{k}\|\mathbf{B}$ shows that the propagation velocity for circular polarized light $c/n_{\pm}$ is different for right- or left-hand polarization. Therefore, a linear polarized light beam, composed of an equal fraction of left- and right-polarized components, experiences a turning of its polarization plane with progressive traveling through a semiconductor sample with a thickness d. The corresponding *Faraday angle* is defined by

$$\theta_F = \frac{\omega d}{2c}(n_+ - n_-) \cong \frac{\omega d}{4c\sqrt{\varepsilon_{opt}}}\left(n_+^2 - n_-^2\right), \tag{63}$$

since $\left(n_+^2 - n_-^2\right) = (n_+ + n_-)(n_+ - n_-) \cong 2\sqrt{\varepsilon_{opt}}(n_+ - n_-)$. The angle can be obtained from Eq. 45 for $\kappa_+^2 \ll n_-^2$ and $\left(\omega_c\tau_{mag}, \omega\tau_{mag}\right) \gg 1$,

$$\theta_F = \frac{360^\circ}{2\pi} \quad \frac{n e^3 B}{m_n^2 \varepsilon_0 \sqrt{\varepsilon_{opt}}\, 2c\left(\omega^2 - \omega_c^2\right)} d \quad \text{for } \omega \gg \omega_c. \tag{64}$$

The quantity $\theta_F/(B\,d)$ is known as the *Verdet coefficient* and is proportional to $n\lambda^2$. The proportionality of the Verdet coefficient with λ^2 is shown in Fig. 10 for n-InSb with the electron density and temperature as the family parameters. It shows an increase of the Verdet coefficient with carrier density in agreement with Eq. 64. It also shows an increase with decreasing temperature due to a temperature-dependent effective mass (see below). With known carrier density, the Verdet coefficient yields the value of the effective mass. The changes in m_n, as a function

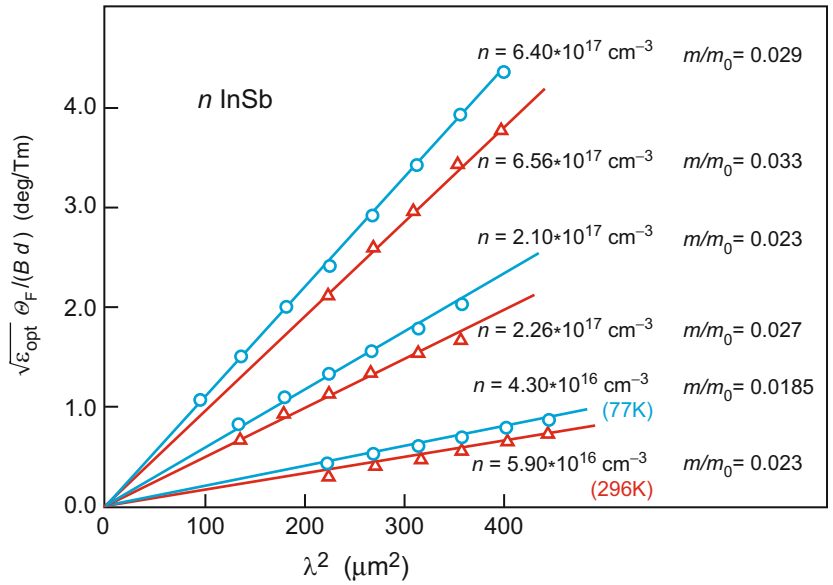

Fig. 10 Faraday rotation in *n*-type InSb with electron density and temperature as parameters; *blue* and *red* curves are for $T = 77$ K and 290 K, respectively. The corresponding average effective mass ratios for the six curves are shown at the *right side* of the figure (After Pidgeon 1962)

of T and n, are due to changes in the electron distribution within the band, indicating that the effective mass increases for electrons higher in the conduction band – see ▶ Sect. 1.2.8 in chapter "Bands and Bandgaps in Solids".

Faraday rotation for electrons is opposite in sign to the rotation for holes. In a multiband semiconductor, both carriers must be considered. For instance, with heavy and light holes, the quantity n/m_n^2 in Eq. 64 must be replaced by $n_{\mathrm{lh}}/m_{\mathrm{lh}}^2 + n_{\mathrm{hh}}/m_{\mathrm{hh}}^2$ for holes.

4 Plasmon Dispersion in 2D Semiconductors

Collective oscillations of carriers (electrons or holes) are altered if they are free to move in two spatial dimensions but have their motion constrained in the third dimension. Two-dimensional plasmons were observed first for electrons on the surface of liquid helium (Grimes and Adams 1976). Most studied two-dimensional free-carrier systems in semiconductors are the two-dimensional electron gas (2DEG) created in semiconductor inversion or accumulation layers of modulation-doped field-effect transistors (Fig. 11a) and multiple layers of 2DEGs, so-called layered electron gas (LEG), realized in modulation-doped multilayer stacks of semiconductor heterojunctions (Fig. 11b). In these structures the free electrons are spatially separated from the ionized donor impurities and

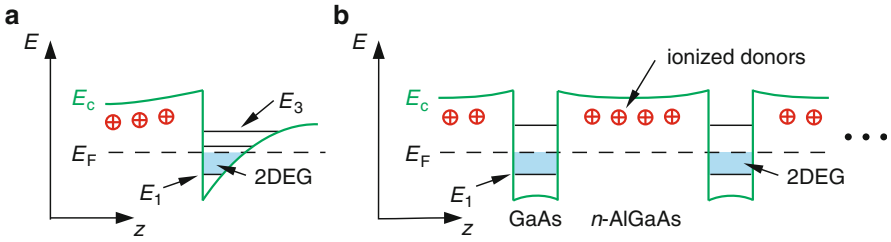

Fig. 11 Two-dimensional electron gas (2DEG) in modulation-doped GaAs/*n*-$Al_xGa_{1-x}As$ structures created (**a**) at the heterojunction and (**b**) in a multi-quantum-well superlattice. E_c and E_F denote the conduction-band edge and the Fermi energy, respectively. Free electrons are confined in the triangular-shaped potential at the interface forming an inversion layer (**a**) or in the undoped GaAs quantum wells (**b**)

scattering by charged impurities is only weak, yielding a high carrier mobility (chapter ▶ "Carrier Transport in Low-Dimensional Semiconductors").

The two-dimensional plasmon resonance of the collective free-carrier motion was calculated for single quantum wells (Stern 1967) and inversion systems (Chaplik 1972), yielding for long wavelengths ($q_{\|} \to 0$)

$$\omega_p^{2D} = \sqrt{\frac{n_{2D}\, e^2}{2\varepsilon_{eff}\, \varepsilon_0\, m_n}}\sqrt{q_{\|}}. \tag{65}$$

with the areal carrier density n_{2D} (in units of cm^{-2}) and the in-plane wavevector of the plasmon $q_{\|}$. ε_{eff} is an effective dielectric function, which accounts for the geometry of the system.[5] Equation 65 shows a square-root dependence on the wavevector for 2D plasmons, in contrast to dispersionless 3D plasmons (Eq. 4).

In a *layered electron gas* with an *infinite* number N of equally spaced 2DEGs according to Fig. 11b the plasma frequency gets (Jain and Allen 1985; Oleg et al. 1982)

$$\omega_p^{LEG} = \left(\frac{n_{2D}\, e^2}{2\varepsilon_{eff}\, \varepsilon_0\, m_n} q_{\|} \frac{\sinh q_{\|} d}{\cosh q_{\|} d - \cos q_{\perp} d}\right)^{1/2} \tag{66}$$

with the normal component $q_{\perp}$ of the wavevector. Equation 66 contains a transition between regimes of different dimensionality. For large separation d between the 2DEG planes ($q_{\|}\, d \gg 1$) the equation reduces to that of a single 2D plama expressed by Eq. 65. For long in-plane wavelengths ($q_{\|}\, d \ll 1$) and in-phase oscillation of all

[5] In single and multiple quantum wells ε_{eff} is the dielectric function of the barriers. In a metal-oxide-semiconductor junction with oxide thickness d_{ox} and perfectly screening gate, $\varepsilon_{eff} = ½(\varepsilon_{semiconductor} + \varepsilon_{ox} \coth(q_{\|}\, d_{ox}))$, see Chaplik 1972.

planes ($q_\perp = 0$) the plasma frequency is similar to that of a 3D system with an electron density n_{2D}/d (Das Sarma and Quinn 1982).

The in-plane wavevector $q_\parallel$ can be varied in inelastic light scattering by changing the angle Θ of the incident light outside the sample with respect to the normal of the sample surface. Choosing the angle between incident and detected backscattered light to 90°, the components of the scattering wavevector are

$$q_\parallel = \frac{2\pi}{\lambda}(\sin\Theta - \cos\Theta) \quad \text{and} \quad q_\perp = \frac{4\pi}{\lambda} n_r \left(1 - \frac{1}{4n_r^2}\right). \tag{67}$$

The resulting dispersion of the 2D plasmon resonance in a layered 2D electron gas (Fig. 11b) is shown in Fig. 12. The dispersion curves indicate the dependence on the sample structure ($q_\parallel d$) and doping (n_{2D}).

In a layered electron gas with a *finite* number N of 2DEG layers, the plasmon resonance is fanned out into a band due to the reduced symmetry (the mirror symmetry at *each* 2DEG is lost) and the Couplomb interaction between the 2DEG layers. A superlattice with N layers has N eigenmodes for the correlated motion of electrons in the different layers. The normal components of the wavevectors for these eigenmodes are given by

$$q_{\perp i} = i\frac{2\pi}{Nd}, \quad i = 1 \ldots N, \tag{68}$$

where d is the superlattice period. $q_{\perp i}\, d$ represents the phase relation beween the layers for the plasmon mode i; for small N the quantity $q_{\perp i}$ loses the physical meaning of a wavenumber.

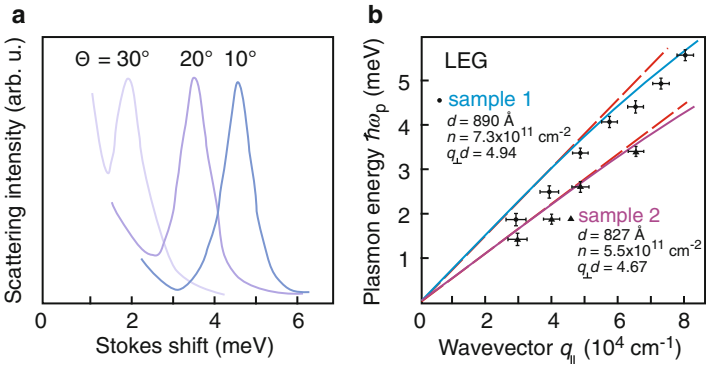

Fig. 12 (**a**) Plasmon Raman line of a layered electron gas (LEG) for different incident angles Θ with respect to the sample normal, yielding different in-plane wavevectors $q_\parallel$. (**b**) Dispersion relation of the 2D plasma frequency for two LEG samples with different electron densities n^{2D} and values of $q_\perp\, d$; upper data points refer to the spectra of panel (**a**). *Solid* and *dashed lines* refer to a calculation according to Eq. 66 and a linear dispersion, respectively (After Oleg et al. 1982)

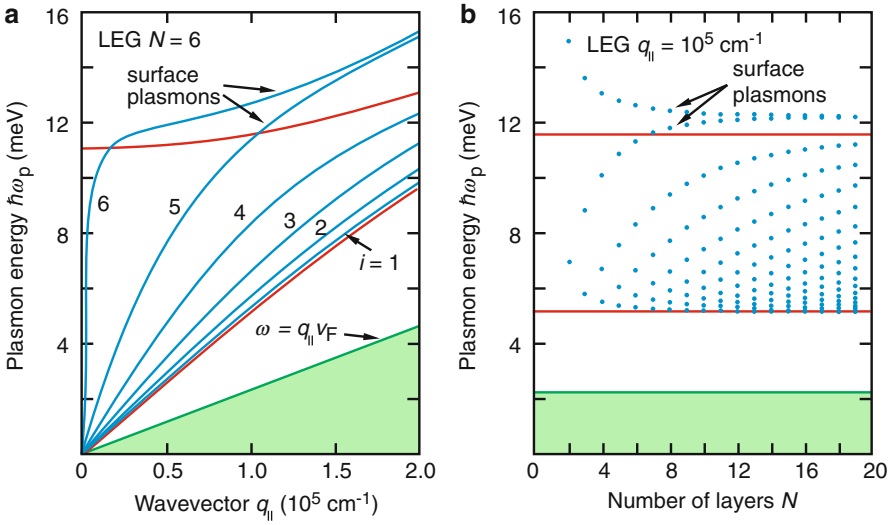

Fig. 13 (**a**) Calculated plasmon energies in a layered electron gas with six 2DEG layers. The *red lines* represent the boundaries of the 3D plasmon band; the *green shaded* area signifies the single-particle continuum. (**b**) Plasmon energies for various numbers N of 2DEG layers in a layered electron gas, calculated for a fixed in-plane plasmon wavevector $q_{\parallel} = 10^5$ cm^{-1} (After Jain and Allen 1985)

The calculated dispersion relation for a layered electron gas with $N = 6$ 2DEG layers is shown in Fig. 13a; the parameters are those of sample 1 in Fig. 12. Each single 2DEG layer has a dispersion $\omega_p \propto \sqrt{q}$, leading to $\omega_p \to 0$ as $q \to 0$ for each branch. In the highest-energy branch electrons in each plane oscillate in phase; for $q_{\parallel} L \ll 1$ the entire layered electron gas of thickness $L = (N\text{-}1)d$ then acts as a single 2DEG layer with an electron density of $N \times n$. The two modes above the 3D plasmon band are surface modes (Giuliani and Quinn 1983). For large values $q_{\parallel} L$ the plasmons on the two outer surfaces do not couple and these modes are degenerate; for small $q_{\parallel} L$ the surface modes split into a symmetric and an antisymmetric mode. We note that the surface modes shown in Fig. 13a lie outside the 3D plasmon band. Such feature originates from a dielectric mismatch between the top and bottom side of the outermost 2DEG layers, if the dielectric constant outsite the superlattice is less than inside. The resulting image charges modify the Coulomb interaction and increase the plasmon energy.

The number of modes increases in a finite layered electron gas as the number of layers N increases as shown in Fig. 13b. The figure also illustrates that the band of the 3D plasmon then becomes gradually more densely populated and eventually continuous for $N \to \infty$; the boundaries of the 3D plasmon are obtained by putting $\cos(q_{\perp} d) = \pm 1$ in Eq. 66.

The discrete plasmon modes were also observed in experiment (Pinczuk et al. 1986; Fasol et al. 1986). A measurement of the plasmon branches in a finite layered electron gas by inelastic light scattering with a GaAs/(AlGa). As sample

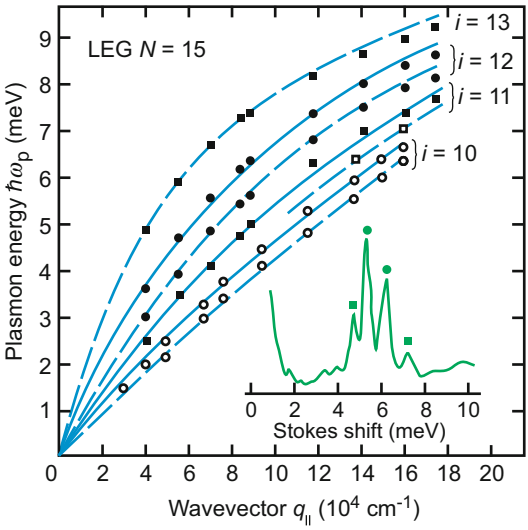

Fig. 14 Experimental plasmon dispersions of a finite layered electron gas with 15 2DEG layers. The *inset* shows the discrete plasmon modes observed in inelastic light scattering for $q_{\parallel} = 8.5 \times 10^4$ cm^{-1}. *Squares* and *circles* indicate weak and strong lines, *filled* and *open* symbols were measured with incident wavelengths of 676 nm and 763 nm, respectively (After Pinczuk et al. 1986)

corresponding to the schematic of Fig. 11b is shown in Fig. 14. Solid and dashed lines represent calculated plasmon energies for antisymmetric and symmetric modes, respectively.

5 Summary

Plasmon oscillations of the free-electron ensemble with respect to the ion cores lead to a resonance absorption in the IR range described by two branches; the plasma frequency depends on the square root of the free-carrier density and represents the low- and high-energy asymptote of the ω_- and ω_+ branches, respectively. An additional resonance absorption occurs at high ($\sim$10 eV) photon energy for valence-electron plasmons. The plasma resonance can be used to determine optically the density, effective mass, and relaxation time of free carriers. The effective mass and its anisotropy can be measured by simple changes of the relative alignment of crystal, electrical, and magnetic fields. The other parameters can often be obtained more easily by electrical measurements; however, optical measurements can be performed when electrical contacts cannot be applied, or electrical measurements are otherwise impeded. If the free carriers are confined to two dimensions the plasmon frequency depends on the in-plane wavevector. In multiple two-dimensional layers of free carriers discrete plasmon branches exist.

Away from the resonance free-carrier absorption and reflection with or without magnetic fields provide also important information about carrier parameters – most significantly about the effective carrier mass, its anisotropy, and its dependence on other variables, such as carrier density and temperature. The knowledge of the effective carrier mass is essential for the analysis of a large variety of semiconducting and electro-optical device properties.

References

Basu PK (1997) Theory of optical processes in semiconductors. Oxford University Press, New York

Cavenett BC, Pakulis EJ (1985) Optically detected cyclotron resonance in a GaAs/$Ga_{0.67}Al_{0.33}As$ superlattice. Phys Rev B 32:8449

Chaplik AV (1972) Possible crystallization of charge carriers in low-density inversion layers. Sov Phys - JETP 35:395

Das Sarma S, Quinn JJ (1982) Collective excitations in semiconductor superlattices. Phys Rev B 25:7603

Dixon JR (1960) Proceedings of 5th international conference physics semicond, Prague, p 366

Drude P (1900) Zur Elektronentheorie der Metalle. Ann Phys (Leipzig) 1:566, and 3: 369 (On the electron theory of metals, in German)

Egerton RF (2009) Electron energy-loss spectroscopy in the TEM. Rep Prog Phys 72:016502

Fan HY (1967) Effects of free carriers on the optical properties. In: Willardson RK, Beer AC (eds) Semiconductors and semimetals, vol 3. Academic Press, New York, p 405

Fasol G, Mestres N, Hughes HP, Fischer A, Ploog K (1986) Raman scattering by coupled-layer plasmons and in-plane two-dimensional single-particle excitations in multi-quantum-well structures. Phys Rev Lett 56:2517

Giuliani GF, Quinn JJ (1983) Charge-density excitations at the surface of a semiconductor superlattice: a new type of surface polariton. Phys Rev Lett 51:919

Grimes CC, Adams G (1976) Observation of two-dimensional plasmons and electron-ripplon scattering in a sheet of electrons on liquid helium. Phys Rev Lett 36:145

Harper PG, Hodby JW, Stradling RA (1973) Electrons and optic phonons in solids-the effects of longitudinal optical lattice vibrations on the electronic excitations of solids. Rep Prog Phys 36:1

Huberman M, Overhauser AW (1982) Open-orbit magnetoresistance spectra of potassium. Phys Rev B 25:2211

Jain JK, Allen PB (1985) Plasmons in layered films. Phys Rev Lett 54:1985

Kaiser W, Collins RJ, Fan HY (1953) Infrared absorption in *p*-type germanium. Phys Rev 91:1380

Kim OK, Bonner WA (1983) Infrared reflectance and absorption of *n*-type InP. J Electron Mater 12:827

Kong X, Albert S, Bengoechea-Encabo A, Sanchez-Garcia MA, Calleja E, Trampert A (2012) Plasmon excitation in electron energy-loss spectroscopy for determination of indium concentration in (In, Ga)N/GaN nanowires. Nanotechnology 23:48

Lax B (1963) Proceedings of international school physics "Enrico Fermi", Course XXII (Smith RA ed), p 240. Academic Press, New York

Maan JC (1993) Intra- and interband magneto-optical properties of bulk semiconductors and heterostructures. In: Martinez G (ed) Optical properties of semiconductors. Springer Netherlands, Dordrecht

Madelung O (1978) Introduction to solid state theory. Springer, Berlin/New York

Mooradian A, McWhorter AL (1967) Polarization and intensity of Raman scattering from plasmons and phonons in gallium arsenide. Phys Rev Lett 19:849

Mooradian A, Wright GB (1966) Observation of the interaction of plasmons with longitudinal optical phonons in GaAs. Phys Rev Lett 16:999

Oleg D, Pinczuk A, Gossard AC, Wiegmann W (1982) Plasma dispersion in a layered electron gas: a determination in GaAs-(AlGa)As heterostructures. Phys Rev B 25:7867

Overhauser AW (1978) Charge-density waves and isotropic metals. Adv Phys 27:343

Palik ED, Furdyna JK (1970) Infrared and microwave magnetoplasma effects in semiconductors. Rep Prog Phys 33:1193

Palik ED, Holm RT (1979) Optical characterization of semiconductors. In: Zemel JN (ed) Nondestructive evaluation of semiconductor materials and devices. Plenum Press, New York, pp 315–345

Palik ED, Wright GB (1967) Free-carrier magnetooptical effects. In: Willardson RK, Beer AC (eds) Semiconductors and semimetals, vol 3. Academic Press, New York, p 421
Palik ED, Teitler S, Henvis BW, Wallis RF (1962) Magneto-optical studies of semiconductors using polarized radiation. In: Stickland AC (ed) Proceedings of 6th international conference physics semicond, Exeter, pp 288–294
Patel CKN, Slusher RE (1968) Raman scattering by polaritons in presence of electron plasma in GaAs. Phys Rev Lett 22:282
Pidgeon CR (1962) PhD thesis, University Reading
Pinczuk A, Lamont MG, Gossard AC (1986) Discrete plasmons in finite semiconductors multilayers. Phys Rev Lett 56:2092
Pines D (1999) Elementary excitations in solids. Perseus Books, Reading
Platzman PM, Wolff PA (1973) Waves and interactions in solid state plasmas. In: Ehrenreich H, Seitz F, Turnbull D (eds). Solid state physics, vol Supplement 13, Academic Press, New York
Poole CP Jr (1998) The physics handbook. Wiley, New York
Roth LM (1982) Dnamics of electrons in electric and magnetic fields. In: Moss TS, Paul W (eds) Handbook of semiconductors, vol 1. North Holland Publishing, Amsterdam
Sakurai JJ, Napolitano J (2011) Modern quantum mechanics, 2nd edn. Addison-Wesley, Boston
Seeger K (1973) Semiconductor physics. Springer, New York
Seeger K (2004) Semiconductor physics, 9th edn. Springer, New York
Stern F (1967) Polarizability of a two-dimensional electron gas. Phys Rev Lett 18:546
Sugano S, Kojima N (eds) (2000) Magneto-optics. Springer, Berlin
Tiginyanu IM, Irmer G, Monecke J, Vogt A, Hartnagel HL (1997) Porosity-induced modification of the phonon spectrum of *n*-GaAs. Semicond Sci Technol 12:491
Wilson JA, DiSalvo FJ, Mahajan S (1975) Charge-density waves and superlattices in the metallic layered transition metal dichalcogenides. Adv Phys 24:17
Wolfe R (1954) On the theory of optical absorption in metals and semiconductors. Proc Phys Soc London Sect A 67:74
Wright GB, Lax B (1961) Magnetoreflection experiments in intermetallics. J Appl Phys 32:2113